Branching Behavior of the Dyonic Multi-Monopole and Multi-Half monopole in the SU(2) Yang-Mills-Higgs Theory

Timothy Tie, Khai-Ming Wong and Dan Zhu

School of Physics, USM Pulau Pinang.

(Received: 31.1.2018 ; Published: 21.11.2018)

Abstract. We studied the branching behaviors of dyonic multi-monopole plus multi-half-monopole for $n = 2,3$ and 4 across $\lambda_b \leq \lambda \leq 25$ at some finite electric charge parameter η where λ_b is the bottom limit of λ. There is only one fundamental solution when $n = 2$. When $n = 3$ and 4, each set of the solutions possesses new branching solutions besides the fundamental one. These branching solutions possess different structures and have higher energies. We investigate on the total energy, E, pole separation, d_z, magnetic moment, μ_m, and electric charge, Q, for different λ.

Keywords: Dyonic, Multi-Monopole and Multi-Half-Monopole, Yang-Mills-Higgs

I. INTRODUCTION

The SU(2) Yang-Mills-Higgs (YMH) field theory has induced a lot of interesting works in formulating magnetic monopole models [1-4]. It is invariant under a U(1) subgroup of the local SU(2) gauge group and undergoes symmetry breaking to give Maxwell's electromagnetic field theory [1]. One of the pioneer works is the t'Hooft Polyakov monopole, a finite-energy and spherically symmetric monopole solution. Such monopole has a topological magnetic charge of $4\pi/e$ [1]. When monopoles superimpose at one location, a multi-monopole with ϕ −winding number equals to n is formed, possesses n topological magnetic charge of $4n\pi/e$ [2]. Exact monopole solutions can only exist within the Bogolmo'nyi-Prasad-Sommerfield (BPS) limit, i.e., when the Higgs self-coupling constant, $\lambda = 0$ [3]. Otherwise, only numerical solutions can be found [5]. Examples of numerical solutions are monopole-antimonopole pair (MAP), monopole-antimonopole chain (MAC) and vortex ring solutions [6,7]. Half-monopole possesses just half of the topological magnetic charge of a t'Hooft Polyakov monopole and has a Dirac string-like singularity along the negative z-axis [8]. The half-monopole co-exists with a t'Hooft Polyakov monopole to form one-monopole plus half-monopole solution [9].

Dyon is a particle possesses fixed magnetic charge and varying electric charge [4]. Every monopole in the SU(2) YMH theory can obtain an electric charge to become a dyonic monopole. Exact dyon solutions were found by Prasad and Sommerfield [3], which were confirmed as Julia-Zee dyon solutions in the BPS limit some time later. The total electric charge and energy of the system approach finite critical values when electric charge parameter, $\eta \to 1$ for the case of non-vanishing Higgs coupling constant, $\lambda \neq 0$. While for the case of $\lambda = 0$, both electric charge and energy of the system approach infinity. Electrically charged half-monopole and one-monopole plus half-monopole were also studied [10]. Branching monopole solutions were found [7] for the

Contributed Paper

electrically neutral MAP and MAC of solutions when $n \geq 3$ and the Higgs self-coupling constant reached a critical value λ_c.

In this paper, we investigate the branching behavior of dyonic multi-monopole and multi-half-monopole when $n = 2,3$ and 4 with Higgs coupling constant $0 \leq \lambda \leq 25$. Vortex rings are obtained when $n \geq 3$. New branching solutions with higher energies than the existing fundamental solution were found when $n \geq 3$ as expected. We calculate numerically for total energy, E, pole separation, d_z, electric charge, Q, and dipole magnetic moment, μ_m, for different λ when $\eta = 0.1,0.5$ and 0.95.

The SU(2) Yang-Mills-Higgs Theory

The Lagrangian in 3+1 dimensions with nonvanishing Higgs potential is shown as follow:

$$L = -\frac{1}{4}F^a_{\mu\nu}\,F^{a\mu\nu} - \frac{1}{2}D^\mu\Phi^a D_\mu\Phi^a - \frac{1}{4}\left(\Phi^a\Phi^a - \frac{\mu^2}{\lambda}\right), \tag{1}$$

where $F^a_{\mu\nu}$ is gauge field strength tensor, $D_\mu\Phi^a$ is the covariant derivative of the Higgs field and λ is the Higgs coupling constant. The term $\mu/\sqrt{\lambda}$ is denoted as ξ and it is the Higgs field expectation value, where μ is the Higgs field mass.

The covariant derivative of the Higgs field and the gauge field strength tensor are given by

$$D_\mu\Phi^a = \partial_\mu\Phi^a + g\varepsilon^{abc}A^b_\mu\Phi^c, F^a_{\mu\nu} = \partial_\mu A^a_\nu - \partial_\nu A^a_\mu + g\varepsilon^{abc}A^b_\mu A^c_\nu, \tag{2}$$

respectively, and the equations of motion are

$$D^\mu F^a_{\mu\nu} = \partial^\mu F^a_{\mu\nu} + g\varepsilon^{abc}A^{b\mu}F^c_{\mu\nu} = g\varepsilon^{abc}\Phi^b D_\nu\Phi^c, D^\mu D_\mu\Phi^a = \lambda\Phi^a(\Phi^b\Phi^b - \xi^2), \tag{3}$$

where the field strength tensor, $F_{\mu\nu}$ [1] is given by $F_{\mu\nu} = \hat{\Phi}^a F^a_{\mu\nu} - \frac{1}{g}\varepsilon^{abc}\hat{\Phi}^a D_\mu\hat{\Phi}^b D_\nu\hat{\Phi}^c = G_{\mu\nu} + H_{\mu\nu}$ where $G_{\mu\nu} = \partial_\mu A_\nu - \partial_\nu A_\mu$ and $H_{\mu\nu} = -\frac{1}{g}\varepsilon^{abc}\hat{\Phi}^a\partial_\mu\hat{\Phi}^b\partial_\nu\hat{\Phi}^c$. The gauge potential $A_\mu = \hat{\Phi}^a A^a_\mu$, where the Higgs modulus is given by $|\Phi| = \sqrt{\Phi^a\Phi^a}$. Such definition of $F_{\mu\nu}$ has a property that the magnetic charge density disappears when $|\Phi| \neq 0$. When $|\Phi| = 0$, there is where the magnetic charge concentrated at. Magnetic field is given by $B_i = \frac{1}{2}\varepsilon_{ijk}F_{jk} = B^G_i + B^H_i$. The net topological magnetic charge and electric charge are given by $M = \frac{1}{4\pi}\int \partial^i B_i d^3x = \frac{1}{4\pi}\oint d^2\sigma_i\, B_i$ and $Q = \frac{1}{4\pi\xi}\int \partial^i E_i d^3x$ respectively. The total energy of the system is given by $E = \frac{g}{8\pi\xi}\int\left\{B^a_i B^a_i + E^a_i E^a_i + D_i\Phi^a D_i\Phi^a + D_0\Phi^a D_0\Phi^a + {}^{\lambda}/_{2}\,(\Phi^a\Phi^a - \xi^2)^2\right\}d^3x$. The electro-magnetic dipole moment can be reduced from the boundary condition of the 't Hooft gauge potential at large r to be $A_i = n(\cos\alpha + \cos\kappa)\partial_i\phi|_{r\to\infty} = -\hat{\phi}_i\mu_m \sin\theta\,/r^2$.

Magnetic Ansatz

The magnetic ansatz used [10]-[11] is given by

$$gA^a_i = -\frac{1}{r}\Psi_1(r,\theta)\hat{n}^a_\phi\hat{\theta}_i + \frac{1}{r\sin\theta}P_1(r,\theta)\hat{n}^a_\theta\hat{\phi}_i + \frac{1}{r}R_1(r,\theta)\hat{n}^a_\phi\hat{r}_i - \frac{1}{r\sin\theta}P_2(r,\theta)\hat{n}^a_r\hat{\phi}_i;$$
$$gA^a_0 = \tau_1(r,\theta)\hat{n}^a_r + \tau_2(r,\theta)\hat{n}^a_\theta; \qquad g\Phi^a = \Phi_1(r,\theta)\hat{n}^a_r + \Phi_1(r,\theta)\hat{n}^a_\theta, \tag{4}$$

where $P_1(r,\theta) = \sin\theta\Psi_2(r,\theta)$ and $P_2(r,\theta) = \sin\theta R_2(r,\theta)$, and $\Psi_1, P_1, R_1, P_2, \Phi_1, \Phi_2, \tau_1$ and τ_2 are the profile functions. The spatial spherical coordinate orthonormal unit vectors are defined

as $\hat{r}_i = \sin\theta\cos\phi\,\delta_{i1} + \sin\theta\sin\phi\,\delta_{i2} + \cos\theta\,\delta_{i3}, \hat{\theta}_i = \cos\theta\cos\phi\,\delta_{i1} + \cos\theta\sin\phi\,\delta_{i2} - \sin\theta\,\delta_{i3}, \hat{\phi}_i = -\sin\phi\,\delta_{i1} + \cos\phi\,\delta_{i2}$. The isospin coordinate orthonormal unit vectors are $\hat{n}_r^a = \sin\theta\cos n\phi\,\delta_{i1} + \sin\theta\sin n\phi\,\delta_{i2} + \cos\theta\,\delta_{i3}, \hat{n}_\theta^a = \cos\theta\cos n\phi\,\delta_{i1} + \cos\theta\sin n\phi\,\delta_{i2} - \sin\theta\,\delta_{i3}, \hat{n}_\phi^a = -\sin n\phi\,\delta_{i1} + \cos n\phi\,\delta_{i2}$. The gauge coupling constant is denoted as g.

The Higgs part of the 't Hooft magnetic field is reduced to $gB_i^G = -n\varepsilon_{ijk}\partial_j\cos\alpha\,\partial_k\phi$ and the gauge part is reduced to $gB_i^H = -n\varepsilon_{ijk}\partial_j\cos\kappa\,\partial_k\phi$, where $\cos\alpha = h_1\cos\theta - h_2\sin\theta$ and $\cos\kappa = (h_1P_1 - h_2P_2)/n$, while $h_1 = \Phi_1/|\Phi|$ and $h_2 = \Phi_2/|\Phi|$.

II. NUMERICAL PROCEDURE

First, we substituted ansatz (4) into equations of motion (3), thus reduce them to 8 coupled non-linear second order partial differential equations. Using Maple and MATLAB software, we solved the PDEs numerically for all space to obtain the solutions for profile functions subject to the fixed boundary conditions when $r \to 0$ and $r \to \infty$ along the z-axis at $\theta = 0$ and π. The imposed boundary conditions at large r are

$$\begin{gathered}\Psi_1(\infty,\theta) = \frac{3}{2}, P_1(\infty,\theta) = n\left[\sin\theta + \frac{1}{2}\sin\frac{\theta}{2}(1+\cos\theta)\right],\\ R_1(\infty,\theta) = 0, P_2(\infty,\theta) = n\left[\cos\theta - \frac{1}{2}\cos\frac{\theta}{2}(1+\cos\theta)\right],\\ \Phi_1(\infty,\theta) = \xi\cos\frac{\theta}{2}, \Phi_2(\infty,\theta) = \xi\sin\frac{\theta}{2}, \tau_1(\infty,\theta) = \eta\xi\cos\frac{\theta}{2}, \tau_2(\infty,\theta) = \eta\xi\sin\frac{\theta}{2},\end{gathered} \tag{5}$$

and the imposed boundary conditions near origin $r = 0$ are

$$\begin{gathered}\Psi_1(0,\theta) = P_1(0,\theta) = R_1(0,\theta) = P_2(0,\theta) = 0,\\ \sin\theta\,\Phi_1(0,\theta) + \cos\theta\,\Phi_2(0,\theta) = 0, \partial_r\left(\sin\theta\,\Phi_1(r,\theta) + \cos\theta\,\Phi_2(r,\theta)\right)\big|_{r=0} = 0,\\ \sin\theta\,\tau_1(0,\theta) + \cos\theta\,\tau_2(0,\theta) = 0, \partial_r\left(\sin\theta\,\tau_1(r,\theta) + \cos\theta\,\tau_2(r,\theta)\right)\big|_{r=0} = 0.\end{gathered} \tag{6}$$

The imposed boundary conditions along the positive z-axis are

$$\begin{gathered}\partial_\theta\Psi_1(r,\theta)|_{\theta=0} = 0, R_1(r,0) = 0, P_1(r,0) = 0, \partial_\theta P_2(r,\theta)|_{\theta=0} = 0,\\ \partial_\theta\Phi_1(r,\theta)|_{\theta=0} = 0, \Phi_2(r,0) = 0, \partial_\theta\tau_1(r,\theta)|_{\theta=0} = 0, \tau_2(r,0) = 0,\end{gathered} \tag{7}$$

and along the negative z-axis are

$$\begin{gathered}\partial_\theta\Psi_1(r,\theta)|_{\theta=\pi} = 0, R_1(r,\pi) = 0, P_1(r,\pi) = 0, \partial_\theta P_2(r,\theta)|_{\theta=\pi} = 0,\\ \Phi_1(r,\pi) = 0, \partial_\theta\Phi_2(r,\theta)|_{\theta=\pi} = 0, \tau_1(r,\pi) = 0 = 0, \partial_\theta\tau_2(r,\theta)|_{\theta=\pi} = 0,\end{gathered} \tag{8}$$

Gauge fixing condition $r\partial_r R_1 - \partial_\theta\Psi_1 = 0$ is applied. The PDEs are next converted into a system of nonlinear equations by using finite difference approximation, then discretized into a grid size of 110×100. The solution grid covers $0 \le x \le 1$ and $0 \le \theta \le \pi$ where $x = r/(r+1)$ is the compactified coordinate. Both g and ξ are set to 1.

III. RESULTS AND DISCUSSIONS

Branching solutions for $n = 2,3$ and 4, $\eta = 0.1, 0.5$ and 0.95 are studied. The introduction of electric charge parameter η indeed produces dyonic monopole solutions. Solutions only available when λ is greater than respective λ_b. Branching happened at some critical value λ_c at $n \ge 3$.

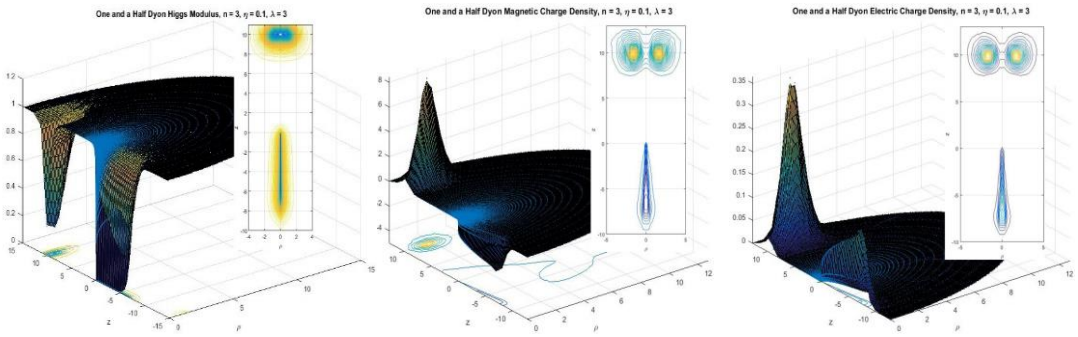

(a) (b) (c)

FIGURE 1. 3D plots of (a) Higgs modulus, (b) magnetic charge density, (c) electric charge density of the dyonic one-monopole plus half-monopole solution when $n = 3, \eta = 0.1$ and $\lambda = 4$.

In FIGURE 1, at some transitional Higgs coupling constant, $\lambda_t > \lambda_c$, the one-dyon does not merge with the one-half-dyon to form a vortex ring but it forms a ring itself, resulting in a dyonic vortex ring and half-dyon solution when $n = 3$ or 4. The vortex ring has a positive magnetic charge and the half-dyon possesses negative magnetic charge, with total magnetic charge of 0, while both having positive electric charges.

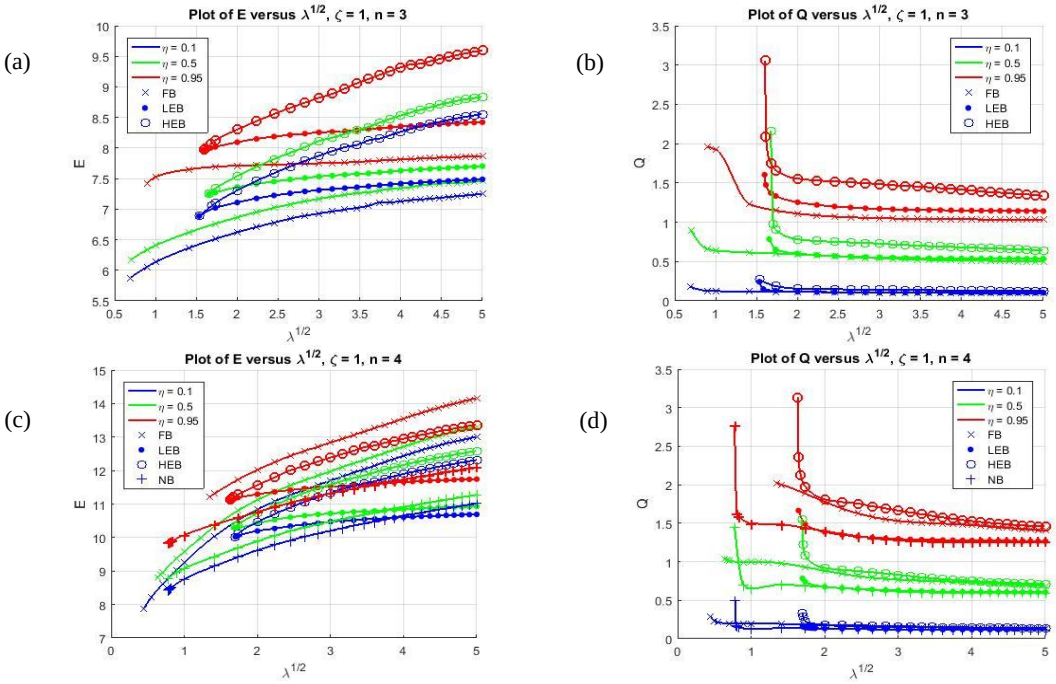

FIGURE 2. Plots of E and Q against $\sqrt{\lambda}$ for (a) and (b) at $n = 3$, (c) and (d) at $n = 4$ respectively.

From FIGURE 2, only fundamental branch (FB) solution is found for each η when $n = 2$. However, the solution has an upper limit at some λ, no further solution can be found. For $n = 3$, two branching solutions denoted as high energy branch (HEB) and low energy branch (LEB) are found. An extra new branch (NB) solutions is found at $n = 4$, which has higher energies than its HEB and has lower λ_b. The FB however, intersects with the LEB at some λ when $n = 4$. As λ increases for $n = 3$ and 4, the total energy E increases and gain saturation, while total electric charge Q decreases and saturates gradually. FIGURE 2(d) and (f) show that Q approaches a very

high value as $\lambda \to \lambda_b$ which is as expected for a dyonic solution, although lower solutions couldn't be found. When $\eta = 0.95$, Q approaches higher value faster. It is noted that the energy branches emerged from the same point at λ_c. While the total electric charge, Q branches emerged from an infinite point. On the other hand, the introduction of η also increases the values of λ_b, λ_c and λ_t as compared to its corresponding electrically neutral configuration.

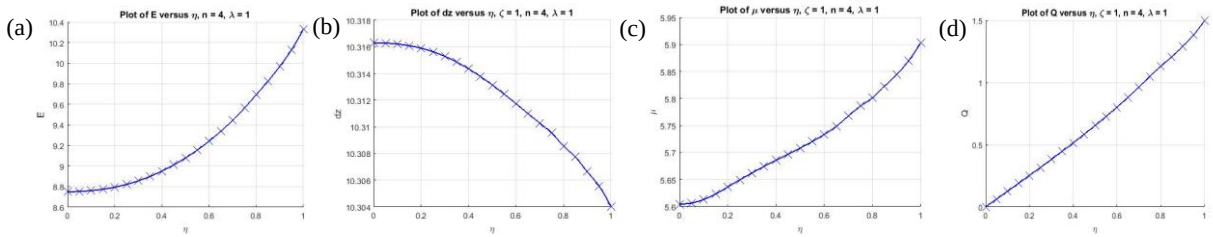

FIGURE 3. Plots of (a) E, (b) d_z, (c) μ_m, and (d) Q against η for the NB solution at $n = 4$.

From FIGURE 3, increment in the electric charge η causes the total energy E, magnetic dipole moment μ_m and total electric charge Q to increase. It is intuitively correct. However, dipole separation d_z decreases in a tiny fraction with increasing η. It is due to the attractive magnetic force between the poles is greater than their repulsive electric force.

IV. CONCLUSION

In the case of dyonic multi-monopole and multi-half-monopole, branching solutions were found when $n \geq 3$ but not at $n = 2$. Vortex ring solution is formed by the multi-monopole when $n \geq 3$. At $n = 3$, a LEB and a HEB solutions are found, emerging from the same point λ_c. It is similar at $n = 4$, with an extra NB solutions which emerged at a lower λ_b. Thus, multi-monopole and multi-half-monopole possesses bifurcating properties similar to multimonopole chain [7]. It is interesting to investigate further the branching behavior of half-monopole in Weinberg-Salam model [12]-[13].

ACKNOWLEDGMENTS

The authors would like to thank School of Physics, Universiti Sains Malaysia.

REFERENCES

1. G. 't Hooft, *Nucl. Phys.* **B79**, 276 (1974); A.M. Polyakov, *Sov. Phys. JETP* **41**, 988 (1975); *Phys. Lett.* **59B**, 82 (1975); *JETP Lett.* **20**, 194 (1974); E. B. Bogomol'nyi and M. S. Marinov, *Sov. J. Nucl. Phys.* **23**, 355 (1976); E. B. Bogomol'nyi, *Sov. J. Nucl. Phys.* **24**, 449 (1976).
2. C. Rebbi and P. Rossi, *Phys. Rev.* **D22**, 2010 (1980); R.S. Ward, *Commun. Math. Phys.* **79**, 317 (1981); P. Forgács, Z. Horváth, and L. Palla, *Phys. Lett.* **99B**, 232 (1981); P. Forgács, Z. Horváth, and L. Palla, *Nucl. Phys.* **B192**, 141 (1981); M.K. Prasad, *Commun. Math. Phys.* **80**, 137 (1981); M. K. Prasad and P. Rossi, *Phys. Rev.* **D24**, 2182 (1981).
3. M. K. Prasad and C. M. Sommerfield, *Phys. Rev. Lett.* **35**, 760 (1975).
4. B. Julia and A. Zee, *Phys. Rev.* **D11**, 2227 (1975).
5. P.M. Sutcliffe, *Int. J. Mod. Phys.* **A12**, 4663 (2013); C.J. Houghton, N.S. Manton, and P.M. Sutcliffe, *Nucl. Phys.* **B507**, 507 (1998).

6. B. Kleihaus and J. Kunz, *Phys. Rev.* **D61**, 025003 (1999); B. Kleihaus, J. Kunz, and Y. Shnir, *Phys. Lett.* **B570**, 237 (2003); *Phys. Rev.* **D68**, 101701 (2003); *Phys. Rev.* **D70**, 065010 (2004).
7. J. Kunz, U. Neemann, and Y. Shnir, *Phys. Lett.* **B640**, 57 (2006).
8. Rosy Teh, B.L. Ng, and K.M. Wong, *Mod. Phys. Letts.* **A27**, 1250233 (2012); *Int. J. Mod. Phys.* **A28**, 1350144 (2013).
9. Rosy Teh, B.L. Ng, and K.M. Wong, *Ann. Phys.* **343 C** (2014).
10. Rosy Teh, B.L. Ng, and K.M. W *J. Phys. G: Nucl. Part. Phys.* **40**, 035004 (2013); *Eur. Phys. J.* **C74**, 2903 (2014).
11. Rosy Teh, A. Soltanian, and K.M. Wong, *Phys. Rev.* **D89**, 045018 (2014).
12. B. Kleihaus, J. Kunz, M. Leibner, *Phys. Lett.* **B663**, 438 (2008); *Phys. Lett.* **B678**, 313 (2010).
13. Rosy Teh, B. L. Ng, K. M. Wong, *Ann. Phys.* **362**, 170 (2015).